Characterization of avalanche loading on impacted structures: a new approach based on inverse analysis

Philippe BERTHET-RAMBAUD,[1,3*] Ali LIMAM,[2] Djebar BAROUDI,[2]
Emmanuel THIBERT,[1] Jean-Michel TAILLANDIER[1]

[1]Erosion Torrentielle, Neige et Avalanche (ETNA), Cemagref, Domaine universitaire, 2 rue de la Papeterie, BP 76,
38400 Saint-Martin-d'Hères Cedex, France
E-mail: rambaud@groupemnd.com
[2]Unité de Recherche en Génie Civil (URGC), Institut National des Sciences Appliquées de Lyon (INSA Lyon),
20 avenue Albert Einstein, 69621 Villeurbanne Cedex, France
[3]Laboratoire Régional des Ponts et Chaussées, Centre d'Étude des Tunnels, 25 avenue François Mitterrand,
69674 Bron Cedex, France

ABSTRACT. Experiments have been conducted on the French full-scale experimental site at Lautaret pass to improve our understanding of the action of snow avalanches on obstacles. The ultimate objective is to provide realistic pressure distribution models suitable for use in civil engineering design and to eliminate the restrictive assumptions currently used in this field. We focus on the feasibility of using the inverse method to quantify the action of the avalanche from its effects on realistic structures rather than from sensors placed directly in the flow. This approach takes into account the interactions between the flow and the obstacle and ensures that the result is effectively the action experienced by the obstacle. The inverse analysis procedure is developed and validated using both numerical and laboratory tests. In situ tests carried out at the Lautaret site to determine the avalanche action at different scales confirm the reliability of this original approach. Its intrinsic characteristics make it especially suitable for application to different structures to provide new knowledge in this complex field.

1. INTRODUCTION

In terms of avalanches, the winter of 1999 was catastrophic in the European Alps, confirming the urgent need to improve the design of avalanche protection structures and buildings subject to snow-avalanche action (Glass and others, 2000). Over the years, civil engineers have continued to improve building design calculations and techniques, developing new tools to take into account complex loading conditions. However, these tools require precise knowledge of avalanche action characteristics. In this paper, we present a new experimental method to determine what structures effectively undergo from a civil engineering point of view when impacted by a snow avalanche.

Many studies have been conducted concerning the action of avalanches on structures (Lang and Brown, 1980; Schaerer and Salway, 1980; McClung and Schaerer, 1985; Schaer and Issler, 2001) and propose pressure measurement methods and values. They correspond mainly to point values measured by pressure sensors impacted by the freely flowing avalanche. Two main limitations make it difficult to use these 'flow' data for civil engineering purposes on the scale of a real structure. First, depending on their size, pressure sensors are often directly subjected to the heterogeneous character of avalanche flow on a decimetric scale, for instance by the impact of snow blocks, resulting in large spatial and temporal variations that are not relevant from a civil engineering point of view. Furthermore, real structures interact with the avalanche, forming an obstacle that creates a stagnation zone and lateral or vertical deviations depending on the structure's behaviour and shape. These interactions are not fully taken

into account by the 'flow' approach, even if recent work (Gauer and others, 2007; Sovilla and others, 2008) provides supplementary data on the spatial variability of the pressure.

However, only a few studies have focused on large obstacles (Kotlyakov and others, 1977; Norem and others, 1985), and, in practice, avalanche experts continue to evaluate avalanche action from the maximum pressure P obtained by a hydrodynamic analogy based on Equation (1) and involving the density ρ and velocity V of the flow (Ancey, 2006):

$$P = k\frac{1}{2}\rho V^2. \tag{1}$$

The k factor theoretically represents the so-called drag factor which depends on the flow regime and obstacle geometry and is used to account for the interaction between the flow and the obstacle. Considering the difficulties in defining and estimating suitable values of V and ρ, which vary with position and time, and the questionable validity of the hydrodynamic analogy, this k factor often becomes a rough safety factor in civil engineering projects (Ancey, 2006). Furthermore, as demonstrated experimentally by Sovilla and others (2008), Equation (1) assumes that the main source of energy in the flow acting on the obstacle is kinetic energy, which may not be true for low-velocity avalanches with Froude numbers near or lower than 1. Under such conditions, the k factor is used to correct any deviation from Equation (1). In addition, Equation (1) provides only a single static pressure value, neglecting the spatial distribution of the pressure and especially its dynamic variation with time which can be crucial to the actual behaviour and strength of rigid structures.

The best way to determine the action of an avalanche on an impacted structure is to introduce a suitable experimental

---

*Present address: MND Engineering, Alpespace, 74 voie Magellan, 73800 Sainte Hélène du Lac, France.

structure in a real path to study the consequences of the avalanche instead of trying to directly measure internal characteristics of the flow such as speed, pressure and density. The main difficulty is that the behaviour of the structure itself inevitably intervenes in the analysis. It is therefore necessary to correctly model this behaviour under complex loading conditions, including dynamic aspects (Berthet-Rambaud and others, 2007).

The final objective of our investigations is to obtain reference data from full-scale avalanche tests to contribute to improved avalanche pressure guidelines including realistic loading scenarios for civil engineers. Furthermore, we believe that quantifying the total response of a structure under loading will provide a basic understanding of flow mechanisms in avalanches. The purpose of this paper is to show the feasibility of the inverse method when applied to in situ avalanche pressure quantification.

2. METHOD

2.1. Experimental and technical constraints

The inverse method requires the introduction of an experimental structure in the avalanche path. The deformation and acceleration of the structure (Fig. 1) measured during the avalanche are used to reconstruct the corresponding loading by inverse analysis. Direct recalculation of these measured values from a numerical model of the structure provides an additional check.

Several aspects must be considered when determining the characteristics of the structure:

The structure must represent the real structure–flow interactions as closely as possible, in particular with respect to the position of the structure facing the avalanche.

The structure must be sufficiently large, in comparison with the representative size of the phenomenon (and its own heterogeneities), to effectively interact with the flow. Two experiments with different geometric characteristics are considered here.

The inverse analysis process introduces further constraints:

The right indicator must be measured as input data for inverse analysis. For example, the analysis of damage caused by real destructive avalanches (Berthet-Rambaud, 2004) provides limited results because only a rough evaluation of the failure pressures can generally be made. To significantly extend the usefulness of results, the behaviour of the structure subjected to the avalanche must be quantified with consistent measurements and measured continuously over time. Hillary and Erwins (1984) have shown that forces reconstructed by inverse analysis using strain gauges are more accurate than those obtained using accelerometers. We therefore use local strain-gauge measurements carried out on our experimental structures for these experiments.

Local measurements have to be converted into resulting avalanche action. This step requires a special study based on inverse problem-solving. Viable experimental structures must be representative of the real situation, but simple enough to allow interpretation of behaviour and application. In particular, a simple geometry must be
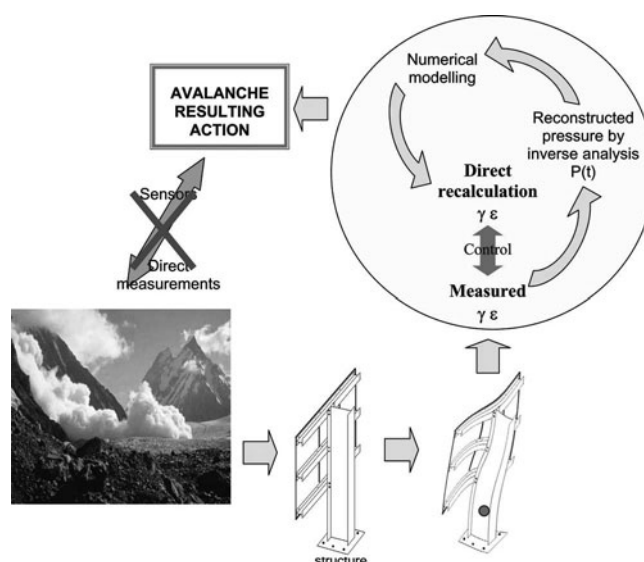

Fig. 1. Applied method based on inverse analysis to measure the action of an avalanche on an impacted structure. Main steps of the inverse analysis procedure including its post-control.

used to ensure unique kinematics and hence few deformation modes.

Finally, the choice of the material is also crucial. Metal structures (steel or aluminium) present many practical advantages such as well-known behaviour and easy characterization by simple laboratory tests. Another advantage of aluminium is the fact that its strain-rate sensitivity is small (of the order of 5%) in the strain-rate range between 10^{-4} and 10^{3} s^{-1} (Langseth and Hopperstad, 1996).

2.2. Full-scale experiments

Site
Experiments are carried out at the Lautaret full-scale avalanche site in the French Alps. This site, owned by the Cemagref research institute, is well known to avalanche specialists for its long experimental history, going back to 1973 (Issler, 1999). Different avalanche paths (Fig. 2) are located on the southeast slope of Mont Chaillol (max. 2600 m a.s.l.) near the Lautaret pass (2058 m a.s.l.).

A reinforced-concrete shelter for data and video acquisition is located between two of the main avalanche paths (1 and 2), which are separated by <20 m. In path 1, a strong concrete foundation was built specifically to support the new experiments. In path 2, a 4.0 m high tripod support is located in the track.

Small to medium avalanches occur at a sufficient frequency (up to three or four each winter). Avalanche flows are generally dense, wet or dry, with sometimes a small but fast powder cloud (or saltation layer). The dense part is usually <1 m thick. The avalanche path is 800 m long with an average gradient of 36° in the experimental zone. Typical release volumes vary from 500 to 10 000 m^3, and maximum front speed can reach 30–40 m s^{-1} (Meunier and others, 2004). Snow deposition by avalanches is therefore limited, and the measurement structures described below are easily cleared of snow and are rapidly operational for the next avalanche release. These conditions make this site of particular interest for experiments involving avalanche impacts on structures.
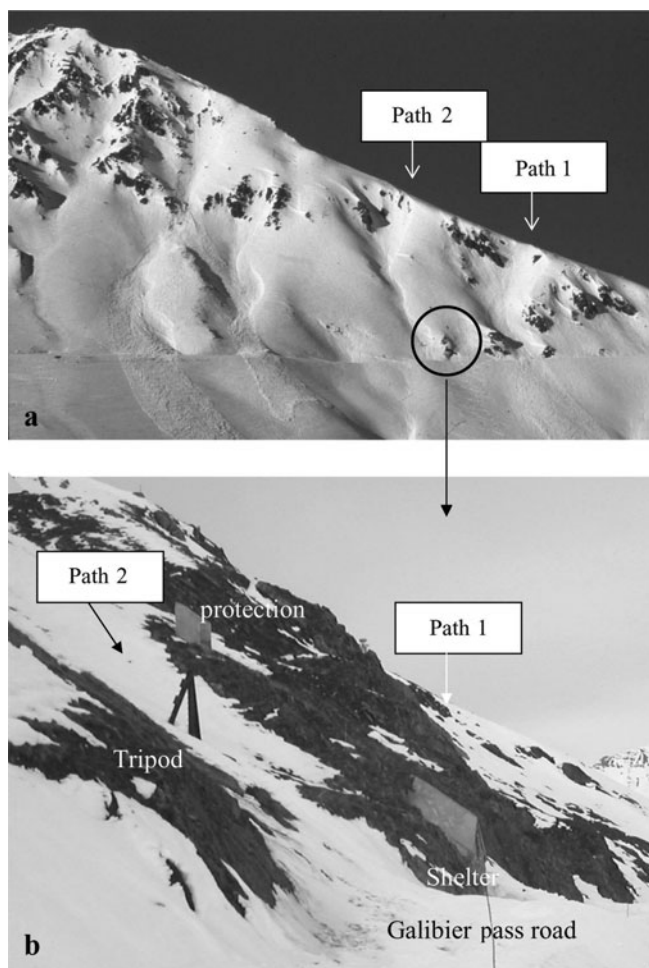
Fig. 2. Lautaret avalanche site with (a) general view of southeast-facing slope of Mont Chaillol and (b) close-up of the experiment area.

Fig. 3. The 1 m² plate at the top of its instrumented support beam in path 1 at Lautaret avalanche site.

Experimental structures and apparatus

Two different experimental set-ups are used. They are both based on the elastic behaviour of metal targets for which deformations are obtained from strain gauges placed at crucial points. Their main difference is the scale:

In path 1, a $1\,\text{m}^2$ plate is supported by a steel beam embedded in the ground and placed normal to the avalanche direction (Fig. 3). This represents a large obstacle in comparison to the flow width (only a few metres at this location) and therefore takes into account the effects of flow heterogeneities. Strain gauges are placed on the beam-reinforced foot in the maximum momentum zone, and a slide system makes it possible to locate the plate exactly at the surface of the initial snow cover prior to avalanche release.

In path 2, small aluminium targets with a plate structure fixed at one end to the wedge and free at the other (Fig. 4) are placed horizontally and normal to the avalanche direction. They are embedded by a rigid cubic piece located between the support and the aluminium plate. These sub-assemblies are bolted at different levels at both sides of the path 2 wedge for easy replacement (Fig. 5). The plate is sufficiently thin to allow cantilever beam behaviour. The width is arbitrarily fixed in a first step, making it possible to consider this target
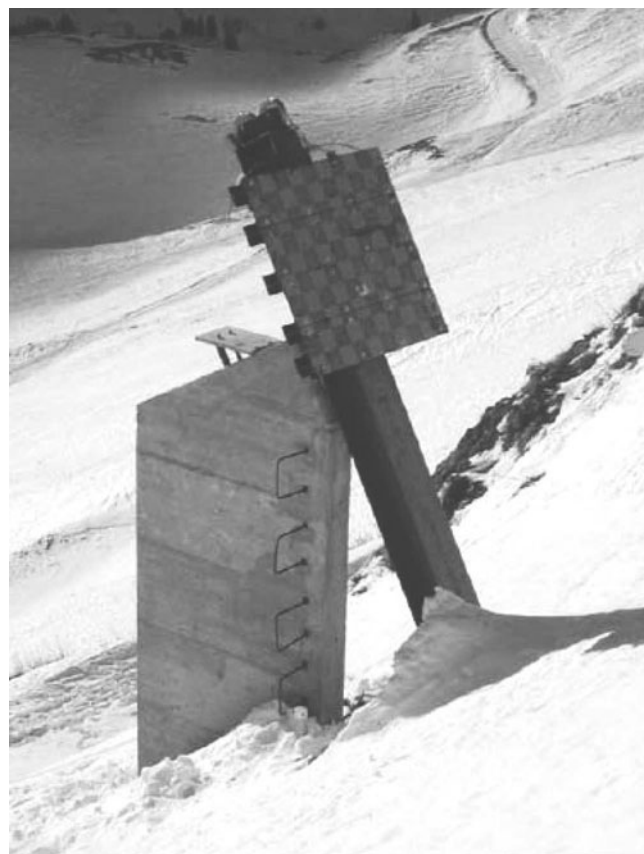
structure as a pressure cell. These very simple devices are dimensioned to have different strengths in order to obtain maximum accuracy depending on their position in the flow (top or bottom) and also to prevent irreversible strains. To monitor the behaviour when subjected to avalanches, a strain gauge is located on the downhill face of the aluminium plate at the location of the potential plastic hinge (1.5 cm from the edge of the embedded zone). The gauge is linked to the data acquisition system in the shelter using a quarter bridge configuration and a frequency of 3000 Hz.

To demonstrate the feasibility of the proposed approach, the next section discusses how these aluminium targets are used. The same concepts apply to the $1\,\text{m}^2$ plate system with equivalent theoretical justification.

3. INVERSE ANALYSIS

3.1. Procedure

A major difficulty of pressure sensors concerns their dynamic calibration and their ability to catch and correctly transcribe pressure peaks. In addition, it is not possible to be perfectly sure that the result actually corresponds to the phenomena to be measured (Gao and others, 2005). Control of the different steps of the inverse analysis procedure allows us to limit such doubt by checking that the evaluated pressure provides the measured local strain by direct recalculation (Fig. 1). Such methods, known as force identification, are widely used in the determination of dynamic loads applied to various structures under unknown loading conditions (Wang, 2002).
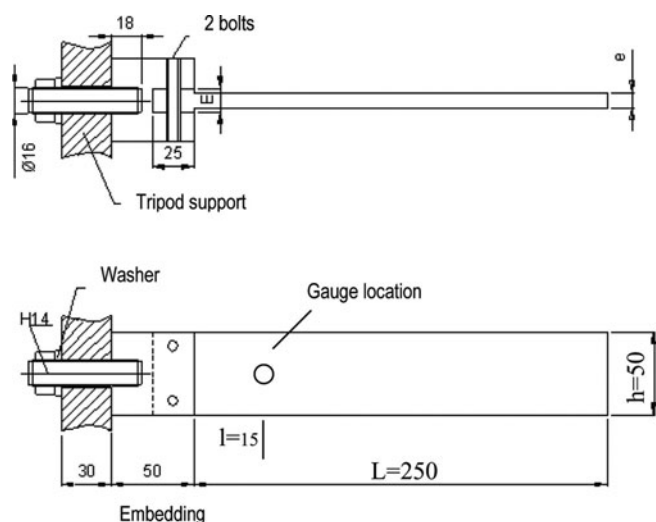
Fig. 4. Aluminium target details (dimensions in mm).

Fig. 5. Aluminium targets on wedge in path 2 at Lautaret avalanche site.

The inverse analysis procedure using local dynamical strain measurements is described here for the aluminium plates. Initially, the avalanche action is assumed to be uniformly distributed over the obstacle. The impacted structure is an elastic cantilever, perfectly clamped at one end and free elsewhere. It is assumed that strains are recorded continuously at known locations. The equations of motion are those of structural dynamics (Gérardin and Rixen, 1993), and an Euler–Bernouilli beam model is used. The elastic assumption can be verified by comparison of the recorded strains with the elastic limit.

Evaluating the strain history from the loading, boundary and initial conditions is the direct problem. Using the Euler–Bernouilli beam model, the direct problem is firstly solved assuming that the impacting force acts at a specific point. It is well established that, in the elastic domain, this formulation is equivalent to solving a Fredholm integral equation of the first order (Meirovitch, 1986):

$$\varepsilon_i(t) = \sum_j \int_0^t h_{ij}(t - \tau) f_j(\tau) \, d\tau, \qquad (2)$$

where ε_i is the strain history measured at point x_i at time t, f_j is the impact load at x_j and h_{ij} is the transfer function between excitation point x_j and point x_i where the strain is measured. The transfer function or its equivalent frequency response function (FRF) in the frequency domain (ω denotes the circular frequency), $\hat{h}(\omega)$, is known once the mechanical model of the structure including its boundary conditions is set. It can be obtained analytically, numerically or experimentally. In this study, the analytical model is corroborated with the experimental model (Fig. 11, shown later).

In parallel, the validity of the Bernouilli–Euler beam model in our 0–1000 Hz bandwidth has been tested by comparing its first five eigenfrequencies with a more sophisticated Kirchhoff thin-plate model using discrete Kirchhoff triangular (DKT) finite elements (Batoz and others, 1980). The finite-element computations were performed using the CASTEM 2000 general purpose finite-element code. The calculated first five frequencies do not differ by more than 1.5% (Table 1).

The associated inverse problem consists of extracting the loading history from the recorded local strain(s) using Equation (2). $f_j(t)$ applied at point x_j is estimated on the basis of the experimental and potentially noisy strain time function $\varepsilon(x_i, t_r)$ at point x_i, recorded at sampling times $t_r \in [0, T]$, $r = 1, 2, \ldots, n$. The frequency domain formulation is used here (Martin and Doyle, 1996; Doyle, 1997). Since the measured signal is discrete, the discrete fast Fourier transform (DFFT) is used (functions under the hat (ˆ) symbol denote the Fourier transform functions of the circular frequency variable ω). The solution $\hat{f}_\delta$ of the inverse problem is given by the regularized deconvolution formula:

$$\hat{f}_\delta(\omega) = \frac{\hat{\varepsilon}_\delta(\omega) \cdot \hat{\phi}(\omega)}{\hat{h}(\omega)}, \qquad (3)$$

where $\hat{\varepsilon}_\delta(\omega)$ is the measured deformation and $\hat{\phi}(\omega)$ is the regularization filter. Such problems are generally ill-posed as presented by Martin and Doyle (1996) and Doyle (1997), so that regularization represented by $\hat{\phi}(\omega)$ is needed to obtain physically meaningful solutions. One specific difficulty is the finite dimension of the structure creating multiple wave reflections superposed on the measured signals. Given that

Table 1. Comparison of the computed eigenfrequencies in bending using an Euler–Bernouilli beam and a Kirchhoff thin plate discretized using DKT finite-elements models

| Mode | Frequency | | Difference |
| | Euler–Bernouilli beam | DKT thin plate | |
	Hz	Hz	%
1	85	84	1.12
2	530	525	0.95
3	1484	1469	1.02
4	2914	2878	1.25
5	4822	4758	1.35

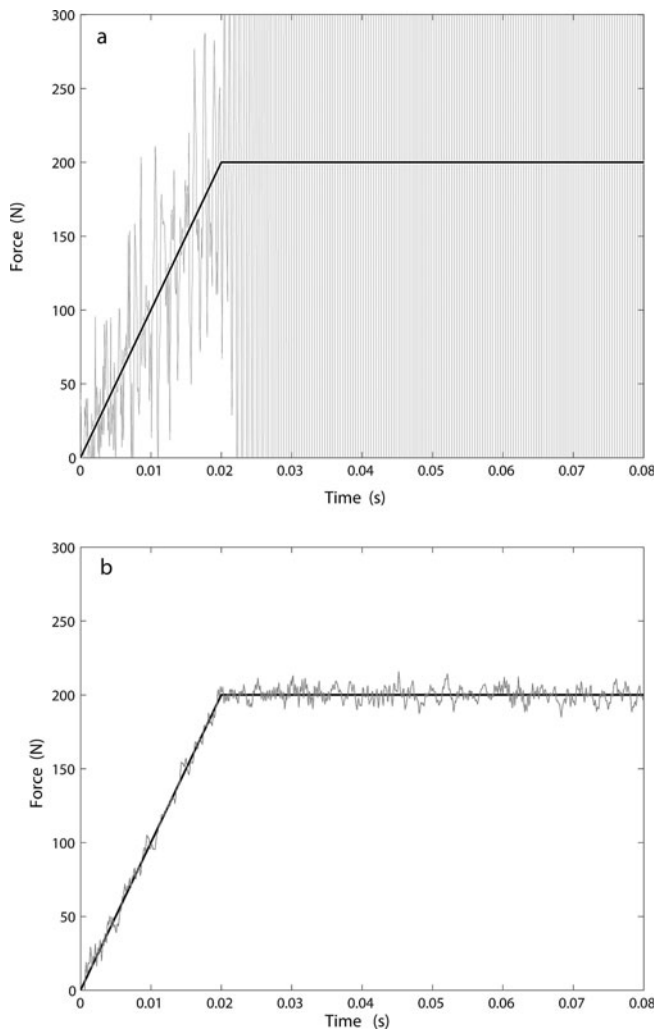**Fig. 7.** L-curve to determine optimal regularization corresponding to ω_c.

Fig. 6. Inverse analysis reconstruction of conventional dynamic loading (step curve) from the corresponding local strain using the beam model and adding a 5% level of Gaussian noise to simulate a real measured strain signal without regularization (a) and with regularization (b).

the FRFs have very small amplitudes near some frequencies, and measured signal ε_δ is polluted by measurement noise, the direct application of the deconvolution formula (Equation (3)) without regularization ($\hat{\phi}(\omega) \equiv 1$) leads to instability of the inverse problem (Tikhonov and Arsenin 1977; Engl and others, 1996). In particular, when $|\hat{h}(\omega)|$ is small (for anti-resonance circular frequencies and for high frequencies), the noise effect becomes predominant and completely pollutes the calculated force in comparison with the regularized force (Fig. 6).

A crucial issue is therefore to find the optimal level of regularization between stability and accuracy. The regularization is obtained here by truncation in the frequency domain (low-pass filter). The filter is such that $\hat{\phi}(\omega) \equiv 0$ above a truncation frequency ω_c and $\hat{\phi}(\omega) \equiv 1$ elsewhere. The optimal truncation frequency ω_c is determined according to the Morozov's discrepancy principle, $\left\| \varepsilon_\omega - \varepsilon_\delta \right\| = \delta$ (Groetsch, 1993; Engl and others, 1996), where δ is the noise level of the measured signal estimated prior to avalanche impact, ε_δ the experimental noisy strain and ε_ω the strain history given by the direct model for a level of regularization corresponding to ω_c. In practice, the observed

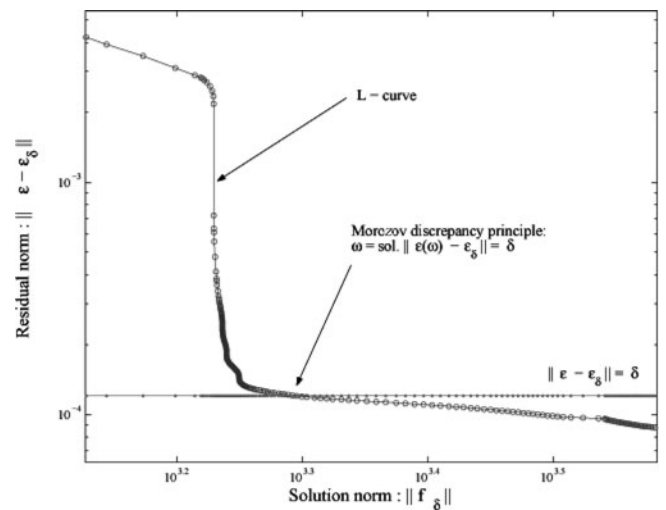noise level did not exceed 1% and the optimal value of regularization is obtained from the L-curve (Tikhonov and Arsenin, 1977; Groetsch, 1993; Engl and others, 1996) which is the graph, parameterized by ω_c, of the norm of the residual vs the norm of the solution in a logarithmic scale (Fig. 7).

3.2. Inverse analysis validation

Dynamic laboratory tests were performed to validate the inverse method before applying it to real strain measurements. The tests consist of impacts by a shock hammer with various impacting heads (rubber, wood, plastic, steel) on aluminium targets equivalent to those used in situ. The advantage of such a device is that both strain and impact force histories can be measured simultaneously to compare measured and reconstructed loads. Strains are measured with strain gauges. According to Doyle (1997), their size together with the density and the Young's modulus of aluminium ensure that the frequency response reaches 300 kHz. The impact load is measured by the piezoelectric force measurement device integrated in the head of the shock hammer (impact-testing device from Bruël & Kjaer, Inc.). The analysis and acquisition system is the DSTP SigLab analyzer 20-42 with a sampling rate of up to 12.8 kHz.

The applied and reconstructed loads are shown in Figure 8. Figure 9 confirms that the first three eigenfrequencies are well reconstructed. The temporal resolution is correct, since the occurrence of the peaks, which correspond to the hammer rebounds on the plate during the manually applied impact, is well represented with time. The amplitude of the peaks is a little lower than that of the measured peaks. This is related partly to the effect of regularization, which introduces more smoothness to the solution, and also to the influence of the hammer impact point which can be quite difficult to locate with precision (Fig. 10). Finally, when the reconstructed load is reinjected into the direct problem, the induced deformations are fully consistent with the experimentally measured values, i.e. within the estimated measurement error (Fig. 11). In summary, the reconstructed load is effectively representative of the load actually applied to the structure, including main dynamic and intensity characteristics.
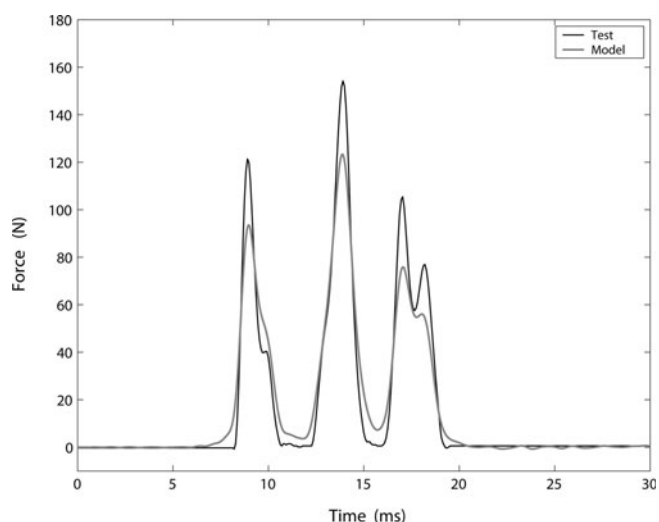
Fig. 8. Comparison of reconstructed and applied loads for a shock hammer test with a 6.51 mm thick aluminium plate impacted by a rubber hammer head.

4. IN SITU RESULTS

Several avalanches have been released at the Lautaret site since December 2002, and two examples are used to illustrate the application of this new approach.

4.1. Avalanche released on 21 February 2006

At the beginning of 2006, snow cover was very low in the Lautaret region, with <30 cm at 2500 m a.s.l. On 16 February 2006, a small atmospheric disturbance reached the Alps and deposited about 30 cm of additional snow on the test site. The Gazex® avalanche release system released only the top 15 cm of the most recent snowfall layer in path 2. When arriving at the wedge, the speed of the flow was about 15 m s^{-1}. This small flow of cold (–2°C) and fine-grained particles of snow (0.3 mm) was dense and included a small saltation layer. The density of the deposit was about 260 kg m^{-3} and included snowballs up to 10 cm in diameter. The measured strain record of aluminium target No. 7 is shown in Figure 12. Before the avalanche was released, this
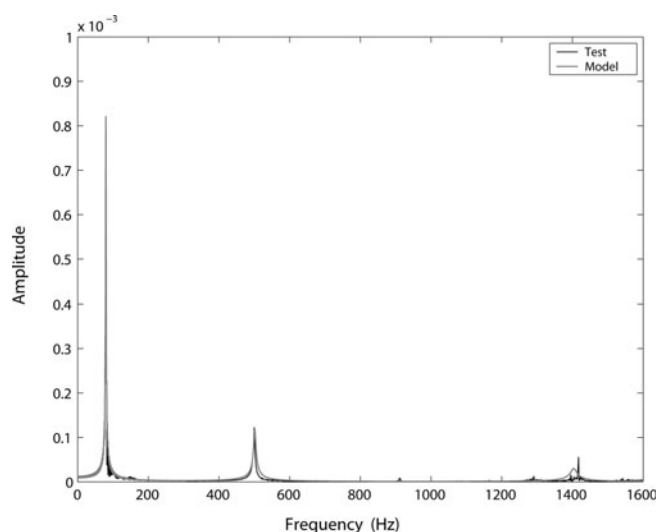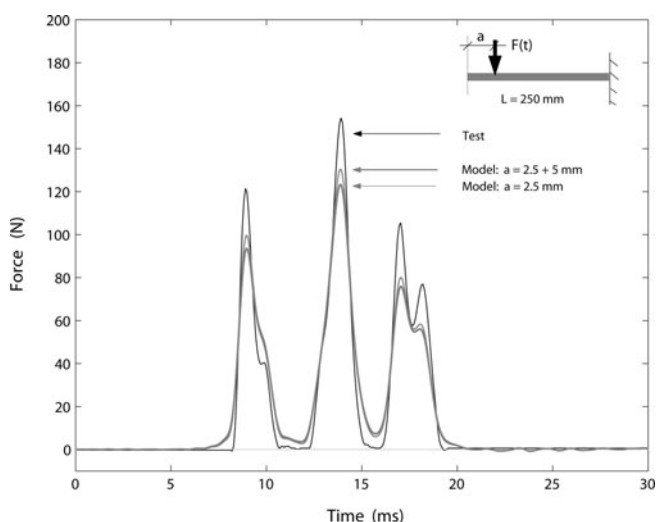

Fig. 10. Influence of the location of the hammer impact point.

target was situated on the wedge, 15 cm above the snow-cover surface (Fig. 5).

The pressure applied on the impacted face of the plate is reconstructed using the inverse method and verifying that the elastic domain has not been exceeded. It is also of interest to compare the result with the simple 'static inversion' (Fig. 13) using the same assumption. This inversion converts strains into pressure, *P*, via their direct relationship in the elastic domain according to:

$$P = \frac{e^2}{3(L-l)^2} E\varepsilon, \qquad (4)$$

where *E* is Young's modulus and ε the deformation (see Fig. 4 for other notations defining the geometrical parameters of the plate). The static inversion cannot distinguish between free oscillations of the plate and forced movements and is consequently insufficient. Free oscillations are incorrectly converted into an oscillating pressure, giving clearly erroneous pressures and even negative values (at about $t = 6$ s), whereas the dynamic inverse method takes into account these free oscillations including inertial forces and evolution with time (dynamics).
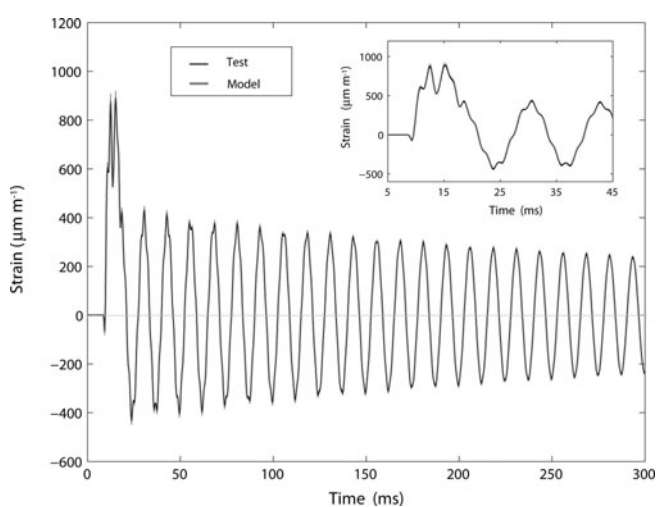

Fig. 9. Theoretical FRFs provided by the beam model compared to shock hammer test measurements.

Fig. 11. Comparison of calculated and measured deformations. The calculated deformations were obtained by reinjecting the deconvoluted force in the direct problem.
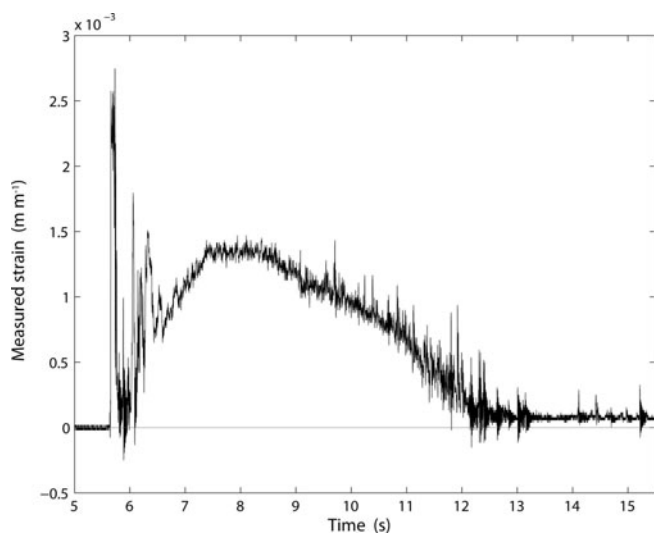
Fig. 12. Measured strains for aluminium target No. 7 with sampling rate of 3000 Hz. Avalanche released on 21 February 2006 on path 2 of Lautaret site.

Fig. 13. Pressure reconstructed by inverse method (with regularization) compared to static evaluation based on Equation (4) for aluminium target No. 7. Avalanche released on 21 February 2006 on path 2 of Lautaret site.

4.2. Avalanche released on 14 March 2006

After the end of February, several snowfalls at the Lautaret site added about 40 cm of fresh and cold snow before the artificial release, with strong wind effects at the top of the paths. The initial density of the snow was 160 kg m^{-3}. The flow was dense and slow and reached the 1 m^2 plate at about 5 m s^{-1} with a thickness of about 70 cm. The plate was located 2.40 m above its base. An accumulation or dead zone appeared rapidly on the uphill side of the plate, resulting mainly in a lateral and partly vertical deviation of the flow due to the presence of the obstacle (Fig. 14). The avalanche decelerated rapidly and stopped after a running distance of 240 m. The density in the deposit was 340 kg m^{-3}, whereas it reached 540 kg m^{-3} in the dead-zone accumulation on the plate.

An equivalent inverse method is used to evaluate the effective action of the avalanche on this obstacle from measured strains (Fig. 15). In order to take into account steel behaviour and strain-rate dependency, an additional damping of 0.33% is added to the analysis. This value is determined using an adapted laboratory dynamic test on a sample of the material. The inverse analysis leads to the results shown in Figure 16 in comparison with different values obtained from current rules and Kotlyakov and others (1977).

4.3. Discussion

Figure 16 shows the reconstruction of the pressure undergone by the structure in the avalanche: this result has to be interpreted in terms of the resultant pressure applied on the whole structure, including indirectly the avalanche and flow characteristics (density, speed, heterogeneity effects, etc.) and the interaction with this structure (stagnation zone, deviation effects, etc.). In this way, this corresponds strictly to the effective loading on the structure, suitable for civil engineering purposes and different from classic pressure measurements (Gauer and others, 2007; Sovilla and others, 2008) which mainly characterize the avalanche flow.

This curve, which constitutes a macro result at the scale of a realistic structure, is of particular interest at different levels:
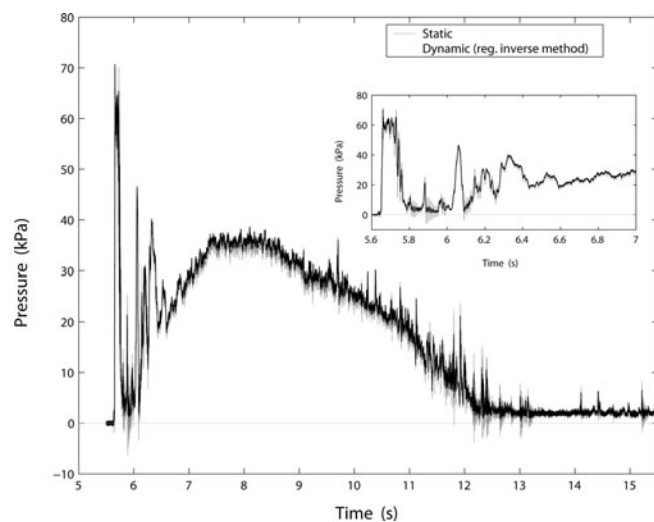
First of all, the resulting pressure with a relatively simple signal appears to be smoother than for aluminium targets due to averaging. Although the aerosol part can potentially generate more disturbed loads, it is obvious that scale aspects greatly influence avalanche pressure measurements with a geometrical averaging in this case. This is totally different from the signal processing often required with pressure sensors to partly eliminate heterogeneity effects. Comparison between measurements made with different scale devices is planned for coming winters, with stainless-steel targets on the 1 m^2 plate coupled with at least one pressure sensor.

Secondly, Figure 16 shows values of the pressure obtained from Equation (1) with $k = 1$, $V = 5$ m s^{-1} and depending on the choice of the density (in the snowpack where the avalanche is released, in the deposit at the bottom of the avalanche track, or in the accumulation zone around the structure). The speed is evaluated from videos which confirm that the flow is almost steady upon impact. The value of 5 m s^{-1} can therefore be considered as an upper limit but not sufficient to explain alone the high pressure level obtained. Using the density of the snowpack before the avalanche ($\rho = 160$ kg m^{-3}) or in the deposits ($\rho = 340$ kg m^{-3}) clearly underestimates the maximum pressure level. Only the value of the density in the dead stopped zone (i.e. outside the theoretical hydrodynamic assumptions) ($\rho = 540$ kg m^{-3}) can give the effective maximum pressure shown in Figure 16. This confirms the limits and the difficulty in using Equation (1) and the current assumptions. In particular, even with $k = 2$, corresponding to the drag factor of a large vertical plate, the initial snow-cover density is still insufficient to reach the maximum measured pressure. Even using the density change proposed by Kotlyakov and others (1977) with $P = \rho_1 \cdot \rho_2 \cdot V^2 / (\rho_2 - \rho_1)$ (where ρ_1 and ρ_2 are respectively the density before and after impact), the value is too low in comparison with the measured maximal value. This last value could be representative of an 'average maximum', but this is not sufficient for the design of civil engineering works. The use of such
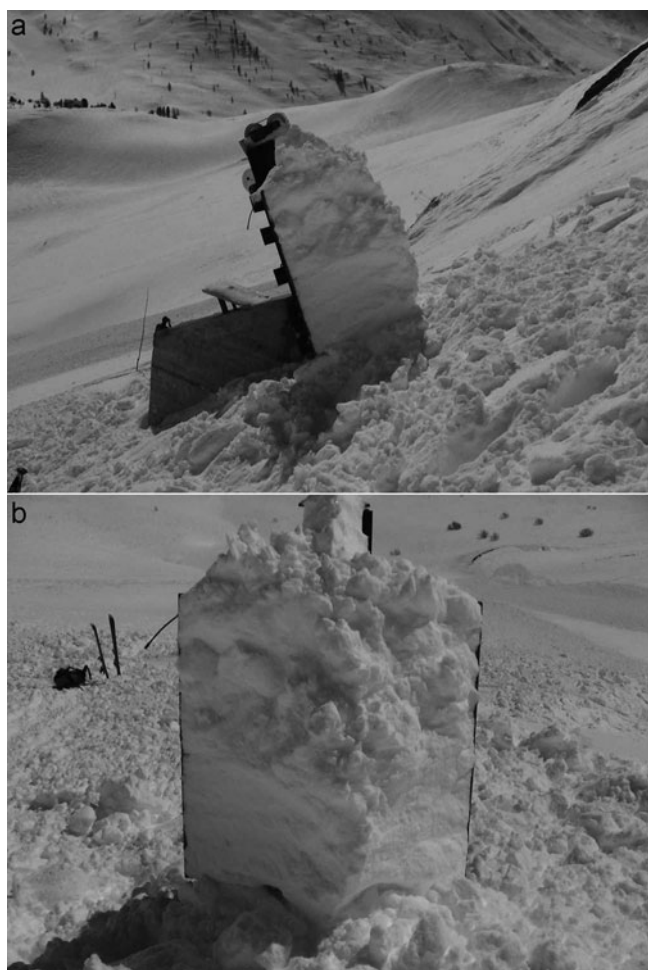
Fig. 14. Accumulation of snow on the exposed side of the 1 m² plate after a dense avalanche on path 1 of Lautaret site. Front and side view.

equations based on a preponderant contribution of dynamics via the square of speed may therefore be subject to question, especially for low-velocity avalanches and consequently for nearly stopped flows. This underestimation of maximal pressure is of particular concern for intermediate-risk (blue) zones where buildings are currently dimensioned with such a formula.

Finally, our results are important mainly in that they quantify the temporal change of avalanche action supported by a full-scale structure for which the size integrates the heterogeneities of the flow. It is also possible to distinguish the impact itself with severe pressure peak(s) and the decreasing step for steady flow. In such a situation, the dynamic change in pressure and its effects on the structure are critical at the time of impact and are absolutely not equivalent to a static load. At the time of the impact, the load increases at a rate of at least 70 kPa s⁻¹. The rate that can be reached in a major phenomenon is still unknown, but it is, for example, assumed to be responsible for the damage to the deflective walls during the Taconnaz avalanche in 1999 (Berthet-Rambaud and others, 2007). The second phase is also of interest. On videos, the dead zone appears rapidly just after the flow impact. It must make a contribution to the overall resistance of this obstacle (structure + dead zone), decreasing to some extent the
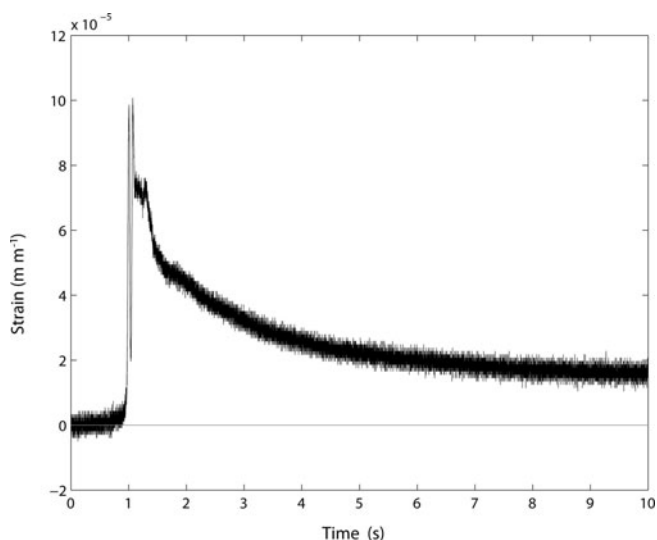

Fig. 15. Measured strains on the beam for the avalanche released on 14 March 2006 on path 1 of the Lautaret site.

pressure against the structure. This overall resistance depends on the geometry of the avalanche front with respect to the geometry, position and shape of the obstacle, which will determine how rapidly the dead zone is created.

5. CONCLUSIONS

The proposed method to evaluate the action of an avalanche on impacted structures focuses on the structure itself, the presence of which is crucial to correctly take into account the interaction between the flow and the obstacle. The sensors are no longer used to measure the pressure of the flow, but rather the consequences (strains or displacements) on a representative experimental structure using strain gauges or accelerometers. The avalanche action is then reconstructed by inverse analysis. Structures are therefore used as macroscopic sensors. The use of two different experimental set-ups at the Lautaret site demonstrates the applicability of this approach. One difficulty is suitable pre-dimensioning of the experimental structures, but this is similar to the problem of choosing the measurement extent,
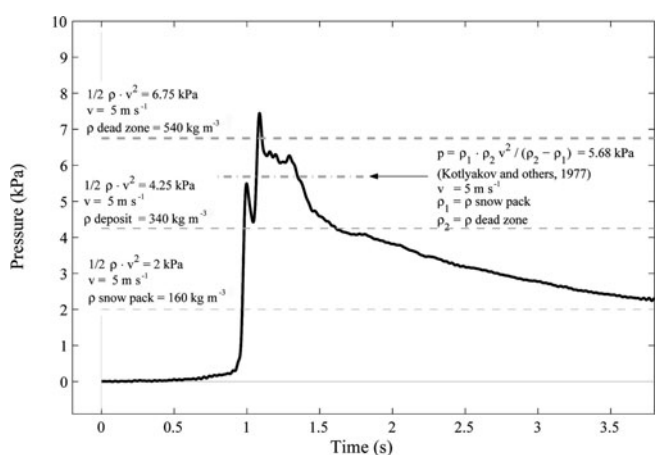

Fig. 16. Reconstructed pressure for avalanche released on 14 March 2006 on path 1 of the Lautaret site.

bandwidth and ultimate strength when using pressure sensors. Concerning the ultimate strength, our devices were dimensioned for a maximal equivalent pressure of 300 kPa, but this limit can be increased easily without an excessive increase in cost. Finally, the main limitation concerns the inverse analysis reconstruction itself. For the time being, it has been developed mainly for bending modes and elastic behaviours, which prevents it from being used on highly complex structures in the flow. Further work is planned to deal with the possible appearance of plastic hinges and irreversible strain. The current small targets could be used to reconstruct the equivalent kinetic energy transmitted to these structures by the flow, rather than an equivalent pressure, which would make it possible to investigate the internal fluctuation of the kinetic energy as postulated by Bartelt and others (2006).

This work was especially aimed at improving current knowledge and practices in the field of structures subjected to avalanches. In particular, our first results suggest that the effective maximum pressure for low-velocity avalanches can be significantly higher than the value calculated using the current approximation based on the hydrodynamic analogy. In addition, the dynamics of avalanche action are confirmed with a possible loading rate of at least $70 \, \text{kPa s}^{-1}$. These two points are already crucial for civil engineers to qualitatively construct and choose representative loading scenarios. Further experiments using this new principle on different test sites will allow the creation of a measurement database which, in conjunction with current developments in granular flows and numerical modelling, should provide a better definition of the action of the reference avalanche in the context of experts' protection studies.

ACKNOWLEDGEMENTS

REFERENCES

Ancey, C., *ed.* 2006. *Dynamique des avalanches.* Lausanne, Presses Polytechniques et Universitaires Romandes; Antony, Cemagref.

Bartelt, P., O. Buser and K. Platzer. 2006. Fluctuation–dissipation relations for granular snow avalanches. *J. Glaciol.,* **52**(179), 631–643.

Batoz, J.L., K.J. Bathe and L.-W. Ho. 1980. A study of three-node triangular plate bending elements. *Int. J. Num. Meth. Eng.,* **15**(12), 1771–1812.

Berthet-Rambaud, P. 2004. Structures rigides soumises aux avalanches et chutes de blocs: modélisation du comportement mécanique et caractérisation de l'interaction 'phénomène-ouvrage'. (PhD thesis, Université Joseph Fourier.)

Berthet-Rambaud, P., A. Limam, P. Roenelle, F. Rapin, J.-M. Tacnet and J. Mazars. 2007. Avalanche action on rigid structures: back-analysis of Taconnaz deflective walls' collapse in February 1999. *Cold Reg. Sci. Technol.,* **47**(1–2), 16–31.

Doyle, J.F. 1997. *Wave propagation in structures: spectral analysis using fast discrete Fourier transforms. Second edition.* New York, Springer Verlag.

Engl, H.W., M. Hanke and A. Neubauer. 1996. *Regularization of inverse problems.* Dordrecht, Kluwer Academic.

Gao, Y., M.J. Brennan, P.F. Joseph, J.M. Muggleton and O. Hunaidi. 2005. On the selection of acoustic/vibration sensors for leak detection in plastic water pipes. *J. Sound Vib.,* **283**(3–5), 927–941.

Gauer, P. *and 7 others.* 2007. On full-scale avalanche measurements at the Ryggfonn test site, Norway. *Cold Reg. Sci. Technol.,* **49**(1), 39–53.

Gérardin, M. and D. Rixen. 1993. *Théorie des vibrations: application à la dynamique des structures.* Paris, Masson.

Glass, B., P. Huet, M. Rat and R. Tordjeman. 2000. *Retour d'expérience sur l'avalanche du 9 février 1999 à Montroc, commune de Chamonix.* Paris, Ministère de l'Ecologie et du Développement Durable. Inspection Générale de l'Environnement.

Groetsch, C.W. 1993. *Inverse problems in the mathematical sciences.* Wiesbaden, Vieweg.

Hillary, B. and D.J. Ewins. 1984. The use of strain gauges in force determination and frequency response function measurements. *In Proceedings of the 2nd International Modal Analysis Conference, 6–9 February 1984, Orlando, Florida,* Vol. 2. New York, The Union College, 627–634.

Issler, D., *ed.* 1999. European avalanche test sites: overview and analysis in view of coordinated experiments. *Eidg. Inst. Schnee-und Lawinenforsch. Mitt.* 59.

Kotlyakov, V.M., B.N. Rzhevskiy and V.A. Samoylov. 1977. The dynamics of avalanching in the Khibins. *J. Glaciol.,* **19**(81), 431–439.

Lang, T.E. and R.L. Brown. 1980. Snow-avalanche impact on structures. *J. Glaciol.,* **25**(93), 445–455.

Langseth, M. and O.S. Hopperstad. 1996. Static and dynamic axial crushing of square thin-walled aluminium extrusions. *Int. J. Impact Eng.,* **18**(7–8), 949–968.

Martin, M.T. and J.F. Doyle. 1996. Impact force identification from wave propagation responses. *Int. J. Impact Eng.,* **18**(1), 65–77.

McClung, D.M. and P.A. Schaerer. 1985. Characteristics of flowing snow and avalanche impact pressures. *Ann. Glaciol.,* **6**, 9–14.

Meirovitch, L. 1986. *Elements of vibration analysis. Second edition.* New York, McGraw Hill.

Meunier, M., C. Ancey and J.-M. Taillandier. 2004. Fitting avalanche-dynamics models with documented events from the Col du Lautaret site (France) using the conceptual approach. *Cold Reg. Sci. Technol.,* **39**(1), 55–66.

Norem, H., T. Kvisterøy and B.D. Evensen. 1985. Measurement of avalanche speeds and forces: instrumentation and preliminary results of the Ryggfonn Project. *Ann. Glaciol.,* **6**, 19–22.

Schaer, M. and D. Issler. 2001. Particle densities, velocities and size distributions in large avalanches from impact-sensor measurements. *Ann. Glaciol.,* **32**, 321–327.

Schaerer, P.A. and A.A. Salway. 1980. Seismic and impact-pressure monitoring of flowing avalanches. *J. Glaciol.,* **26**(94), 179–187.

Sovilla, B., M. Schaer and L. Rammer. 2008. Measurements and analysis of full-scale avalanche impact pressure at the Vallée de la Sionne test site. *Cold Reg. Sci. Technol.,* **51**(2–3), 122–137.

Tikhonov, A.N. and V.Y. Arsenin. 1977. *Solutions of ill-posed problems.* Washington, DC, V.H. Winston and Sons; New York: Wiley.

Wang, B.-T. 2002. Prediction of impact and harmonic forces acting on arbitrary structures: theoretical formulation. *Mech. Syst. Signal Process.,* **16**(6), 935–953.